NJC

ROYAL SOCIETY OF CHEMISTRY

PAPER

View Article Online
View Journal | View Issue

Cite this: *New J. Chem.*, 2026, **50**, 4768

Green synthesis of glycerol carbonate using efficient mixed oxide catalysts

Linda Miturova, Ivonne Rodriguez-Donis and Pascale de Caro*

Received 2nd September 2025,
Accepted 12th January 2026

DOI: 10.1039/d5nj03530a

rsc.li/njc

The transcarbonation reaction of glycerol (Gly) with diethyl carbonate (DEC) was investigated to synthesise glycerol carbonate (GC) using two major types of basic catalysts: conventional carbonates (K_2CO_3 and Na_2CO_3) and, for the first time in this context, metal oxides (CaO, MgO, MgO/CaO and KNO_3/CaO) calcined at 700 or 900 °C. The introduction of metal oxides as catalysts represents a novel approach for this type of transcarbonation reaction. Analyses showed that the mixed CaO based metal oxides have a porous structure suitable for the transcarbonation reaction and higher BET surface areas compared to single CaO oxide. Two different loadings of each catalyst (5 and 10% mass related to Gly) were used with 2 : 1 molar excess of DEC to produce GC during 3 hours at 110 °C under mechanical stirring (500 rpm). The results showed the benefit of using mixed oxides (MgO/CaO or KNO_3/CaO) calcined at the appropriate temperature, to obtain GC yields and selectivity higher than 90% without byproduct formation.

1. Introduction

Faced with increasing global demands for cleaner energy sources, biodiesel is still considered a useful biofuel when blended with commercial diesel fuel. The usual way to produce biodiesel is *via* the transesterification reaction of animal or vegetable oils with an alcohol, to obtain fatty acid methyl esters (FAMEs). Glycerol as a main co-product represents 10% of the biodiesel production.[1,2] Its valorisation is crucial to ensure the competitiveness of the production chain. So, glycerol is an available polyol with interesting properties for numerous industrial fields such as the pharmaceutical and food industry. It is also a platform molecule for the chemical industry, to prepare new valuable chemicals.[3,4]

Glycerol carbonate (4-hydroxymethyl-1,3-dioxolan-2-one) is one of the most significant derivatives of glycerol. Glycerol carbonate (GC) is a non-toxic, biodegradable molecule, stable over a wide range of temperatures, with a boiling point of 353 °C at atmospheric pressure and a melting point at −69 °C. It is considered an attractive substitute for various synthetic derivatives for many applications. For instance, GC is commonly used as an alternative solvent for nail polish remover and for gas separation membranes, as a humectant for pharmaceuticals or as a plasticizer.[4,5] Currently, GC is providing great interest as an electrolytic component of lithium batteries.[6] In comparison with other carbonate-based solvents, GC has a high dielectric constant[4,7] and the ability to form a solid layer of oligomer on the interface between the electrode and electrolyte, thus generating a passivation effect and enhancing the lifetime of the lithium cell.[4,8] The ambivalent character of glycerol carbonate, due to the primary hydroxyl group and the 2-oxo-1,3-oxolane group (ODO), confers a large chemical reactivity to the molecule.[4,8] Indeed, it is an intermediate for the synthesis of esters,[9,10] biobased polyhydroxyurethanes,[11] polyglycerols[12] and poly(glycerol carbonates).[12]

Various methods for the synthesis of GC from glycerol have been investigated. Direct carbonation of glycerol using phosgene presents disadvantages in terms of safety and the environment.[4,13] The two step production of GC can be conducted using ethylene oxide reacting directly with CO_2 and glycerol to form GC. This route displays some thermodynamics limitations as well as the employment of a toxic ether revealing security constraints.[14] Today, the reaction of glycerol with urea is one of the most studied routes of synthesis. However, this reaction involves high reaction temperatures[15,16] and the formation of biuret and isocyanic acid, both toxic. Furthermore, the most common catalysts are organometallic sulphates,[17] prepared with sulphur dioxide considered toxic to aquatic environments.[18]

Finally, the possibility of obtaining glycerol carbonate from glycerol *via* a transesterification reaction with a carbonate source offers good prospects. Dimethyl carbonate (DMC) has been commonly used as a source of carbonate combined with homogeneous or heterogenous catalysts for selective transcarbonation.[19–23] Under these conditions, the transcarbonation reaction of glycerol to produce GC leads to a co-product, methanol, which forms an azeotropic mixture with DMC,

Laboratoire de Chimie Agro-Industrielle, LCA, Toulouse INP, Université de Toulouse, France. E-mail: pascale.decaro@ensiacet.fr

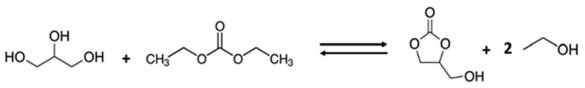

Fig. 1 Transcarbonation reaction of glycerol and DEC to produce GC and ethanol.

making its separation difficult and costly.[24–26] Therefore, the objective of the present work is to investigate the use of diethyl carbonate (DEC) to replace the DMC as the carbonate source. This alternative pathway generates ethanol as a co-product without forming an azeotropic mixture with the reactant DEC.[27] The scheme of the reaction is presented in Fig. 1. The transcarbonation reaction involves two successive nucleophilic attacks of the primary and secondary hydroxyl groups of glycerol on dialkyl carbonate, leading to the departure of the corresponding alkoxide ion. With diethyl carbonate, ethanoate ions are released, but methanoate is a better leaving group compared to ethanoate,[28] as the latter is destabilized by the higher electron density on its partially negatively charged oxygen atom. The removal of high purity ethanol during the reaction is possible, as it is the most volatile component of the system, which also helps shift the equilibrium towards the formation of the desired product. The employment of a DMC substitute for the transcarbonation reaction of glycerol has rarely been reported in the literature and is typically associated with the use of complex catalysts containing rare metals. For example, studies using Mg/Al based catalysts (hydrotalcite-like compounds) have been reported, although they require long reaction times, reaching only 76% yield after 50 hours of reaction at 130 °C[29] or 80% of glycerol conversion after 8 hours at 130 °C.[30] Souza Junior *et al.* (2023) tested a Ca/Al based catalyst in the presence of DMSO, achieving a 91% yield of glycerol carbonate after 5 hours at 130 °C.[31] CeO_2 based catalysts mixed with Ni oxide were used by Wu *et al.* (2017), for the synthesis of CG from DEC, with 94% glycerol conversion and GC selectivity of 90.95% after 8 hours at 85 °C.[32] Andola *et al.* (2025) have recently synthesised GC from glycerol and DEC by adding 20% of $NaAlO_2$ catalyst prepared by spray drying and sonication methods, using a glycerol-F127 template to increase its surface area. In their work, a large excess of DEC was used (1 : 4 molar, Gly : DEC) at 90 °C, to obtain 92% of Gly conversion and 100% of GC selectivity after 3 hours, using the complex $NaAlO_2$ catalyst system.[33]

So, the present study involves the screening of readily available catalysts, such as oxides and carbonates of alkaline earth and alkali metals, to develop efficient conditions for the production of glycerol carbonate (GC) *via* the transcarbonation reaction of glycerol and diethyl carbonate (DEC) in 3 hours at 110 °C. The performances of catalysts are compared in terms of glycerol conversion, GC yield, and selectivity. To our knowledge, such catalysts have never been studied for this chemical route. Some of these catalysts have already been tested for the transesterification reaction of glycerol with DMC.[3,34] The choice of the catalyst focuses on three main criteria: high activity, chemical stability and cost. We selected two earth metal carbonates (K_2CO_3 and Na_2CO_3), two metal oxides (CaO and MgO), and mixed metal oxides based on an active calcium oxide core (MgO/CaO and CaO mixed with potassium cations using the KNO_3/CaO catalyst). The study also aims to understand which characteristics of these catalytic systems are crucial to improve the performance of the transcarbonation reaction when replacing DMC by DEC. Therefore, the preparation of the heterogeneous catalysts and their characterisation are preliminary steps.

2. Experimental methods

2.1. Materials and chemicals

Anhydrous glycerol (high purity of ≥99%) was supplied by Reagent Plus, Sigma (USA). Anhydrous diethyl carbonate (DEC) of purity 99% was obtained from Thermo Fisher Scientific (USA). HPLC isocratic grade absolute anhydrous ethanol was obtained from CARLO ERBA Reagents (Italy). The catalysts, K_2CO_3 ACS reagent, ≥99.0% and Na_2CO_3 99%, were supplied by Sigma (USA). The metal oxides MgO 95% and CaO, reagent grade, were obtained from Sigma (USA). No further treatments were applied to the reagents mentioned previously.

Standard quality glycerol carbonate (GC) was supplied by Huntsman (USA) and purified using thin film evaporation to obtain the final purity of 95–98%. Ion exchange resin Amberlite 120H R was supplied by Sigma (USA). HCl, 36% used to regenerate the resin was obtained from Thermo Fisher Scientific (USA).

2.2. Preparation of simple and mixed oxide catalysts

2.2.1. Preparation of homogeneous catalysts. Sodium carbonate and potassium carbonate were both dried at 105 °C under static air for at least 4 hours before the experiments. They were both stored in a desiccator under reduced controlled humidity, maintained between 20 and 29% depending on the temperature, which varied from 16 to 27 °C.

2.2.2. Preparation of simple and mixed heterogeneous catalysts. Magnesium and calcium oxide were calcined in an air furnace at 800 °C for 3 hours before being used for the reaction. For the preparation of mixed oxide MgO/CaO, individual metal oxides were previously calcined at 550 °C for 12 hours, followed by sieving through 1 mm mesh. Then the mixed metal oxide catalyst was prepared by mechanical mixing of MgO and CaO, with the mass ratio of metal ions Ca^{2+} : Mg^{2+} of 1 : 1.1, according to the adapted protocol of Khayoon and Hameed (2013).[3] The mixture was calcined at 800 °C, then sieved through 500 μm mesh and stored in a desiccator.

The mixed metal oxide catalyst KNO_3/CaO was prepared by dry impregnation. First, CaO was dried at 105 °C during 4 hours, then calcined in an air furnace at 550 °C for 12 hours to remove the physiosorbed water and activate the catalyst. Then, it was mixed with an aqueous solution of KNO_3 prepared as follows: 2.15 g of KNO_3 were dissolved in 25 mL of distilled water, according to the protocol of Hu *et al.* (2015).[34] The solution was homogenised *via* ultrasound treatment and

stirred at room temperature for 10 min. Then 10 g of the calcined CaO powder were added, and the mixture was stirred for 15 min and set to equilibrate for 48 hours at ambient temperature. Subsequently, the mixture was dried at 105 °C for 24 hours and calcined under static air at 700 °C for 5 hours (KNO_3/CaO 700) and 900 °C for 3 hours (KNO_3/CaO 900), using the heating ramp of 2.5 °C min^{-1}. The prepared mixed catalysts were sieved at 500 μm mesh and stored in desiccator. Before their use, the catalysts were dried at 105 °C for 4 hours, to remove the possible remaining physisorbed water.

2.3. Catalyst characterisation

2.3.1. Inductively coupled plasma – atomic emission spectroscopy (ICP-AES). The samples were analysed using an iCAP 6300 thermo generator RF equipped with a CID optical detector (LCC, Toulouse, France). The mineralization was performed using a mixture of HNO_3 and HCl (1 : 3 v/v) for 1 hour. Mg, Ca and K contents were determined.

2.3.2. X-ray diffraction. X-ray diffraction patterns of simple or mixed metal oxide catalysts were recorded on a Rigaku Miniflex 600 powder diffractometer in the $\theta/2\theta$ configuration, equipped with a Cu anode X-ray tube and a HyPix 400 MF 2D hybrid pixel detector. The diffractograms were processed using the Panalytical Highscore+ software. Results were compared with data from the crystallography open database (COD).

2.3.3. Fourier transform infrared spectroscopy. Fourier transform infrared spectroscopy FT-IR spectrometer: Perkin-Elmer Spectrum 65 (Walthan, MA, USA) was used at room temperature over a frequency range of 4000 to 400 cm^{-1} with a resolution of 4 cm^{-1} and 64 scans. KBr pellets (300 mg, dried at 105 °C for 12 hours and stored in a desiccator) were used as the support medium for analyses.

2.3.4. Scanning electron microscopy (SEM). The surface morphology of metal oxide catalysts was studied with a Quanta 450 scanning electron microscope (Hillsboro, OR, USA) operating at 5 and 15 kV, under a partial water pressure of the chamber of 130 Pa with high vacuum mode.

2.3.5. Brunauer–Emmett–Teller (BET) surface analysis. The total surface area, pore volume, and average pore diameter of the catalyst were studied using an N_2 physisorption analyser, a TriStar II device from (Micromeritics, USA). Nitrogen adsorption/desorption isotherms were measured at −195.8 °C (CIRIMAT, Toulouse University). Prior to analysis, catalyst samples were degassed with N_2 at 100 °C for 3 hours. The BET method was used to determine the specific surface area of catalysts at the relative pressure (p/p_0) range of 0 to 1. The Barrett–Joyner–Haleda (BJH) method was used to calculate the pore size distribution, from the adsorption isotherms.

2.3.6. Thermogravimetric analysis (TGA). The thermal stability of metal oxides was studied using Mettler Toledo TGA 2 (Mettler Toledo, Greifensee, Switzerland) under a nitrogen atmosphere from 25 to 1100 °C with a heating rate of 5 °C min^{-1}, followed by an isotherm at 1100 °C for 10 min.

The thermal decomposition study of pure KNO_3 was carried out on a Mettler Toledo TGA/DSC 3+ Thermal Analysis system (Mettler Toledo, Greifensee, Switzerland) by mimicking the conditions used during the calcination of the KNO_3 900 catalyst under a nitrogen atmosphere from 25 to 900 °C with a heating rate of 5 °C min^{-1}, followed by an isotherm at the maximum temperature for 3 hours.

2.3.7. Basic strength evaluation by the Hammett indicator method. The basicity of the catalyst was determined using the Hammett indicator method, adapted from the procedure reported by Hu *et al.* (2015).[34] The basic strength of each catalyst was characterised on the Hammett scale using a series of colour indicators: phenolphthalein (H_ = 9.3), 2,4-dinitroanilline (H_ = 15.0), 4-nitroaniline (H_ = 18.4) and aniline (H_ = 27.0).

Prior to the basicity measurements, each catalyst sample was dried at 105 °C for 3 hours. Subsequently, 1 g of the dried catalyst was dispersed in pure cyclohexane, and a few drops of the indicator solution (0.5 wt% Hammett indicator dissolved in toluene) were added to the suspension. After 2 hours of contact, the colour changed of the mixtures was observed visually to determine the corresponding basicity.

2.4. Catalytic reaction

The transcarbonation reaction was conducted in a 250 mL batch reactor equipped with a double jacket, connected to a silicone oil thermostatic bath, which was used to maintain a constant reaction temperature. In the reactor, 10 g of glycerol were mixed with 25.66 g of DEC, corresponding to a Gly : DEC molar ratio of 2 : 1. Either 0.5 or 1.00 g of catalyst (5 and 10 wt% relative to glycerol) was added. The mixture was then heated at 110 °C and stirred mechanically at 500 rpm for 3 hours. Two experimental trials were conducted for each catalyst to verify the repeatability of the results. After completion of the reaction, the reactional medium was cooled and the catalyst was separated either through cationic filtration resin for the compounds displaying homogenous behaviour, or by centrifugation (5 min, 20 °C, 3800 g force) for the heterogeneous catalysts. Finally, the distillation under reduced pressure was used to evaporate the most volatile compounds (formed EtOH and remaining DEC) contained in the filtrate and supernatant.

2.5. Product analysis

The final product was analysed by gas chromatography (GC-FID) with an automatised injection workstation (Varian 3900), equipped with a CP-WAX 52 CB WCOT fused silica column and a flame ionization detector (GC-FID). Samples were diluted in ethanol with a dilution factor ranging from 20 to 180 in order to respect the maximum saturation concentration. The tetra(ethylene glycol) (TEG) was used as the internal standard. The carrier gas used was helium at 1.2 mL min^{-1}. The injector split ratio was 80 and the temperature was 220 °C. The oven temperature was initially set at 60 °C (1 min) followed by ramping at a rate of 20 °C min^{-1} to 240 °C and it was then held at this temperature for 5 min. The FID temperature was maintained at 250 °C.

The following equations, eqn (1)–(3), were used to calculate glycerol conversion (conversion Gly), glycerol carbonate yield

(yield GC) and glycerol carbonate selectivity (selectivity GC).

$$\text{Conversion Gly}\ (\%) = \frac{\text{moles of Gly}_{\text{initial}} - \text{moles of Gly}_{\text{unreacted}}}{\text{moles of Gly}_{\text{initial}}} \times 100 \quad (1)$$

$$\text{Yield GC}\ (\%) = \frac{\text{moles of GC}_{\text{produced}}}{\text{moles of Gly}_{\text{initial}}} \times 100 \quad (2)$$

$$\text{Selectivity GC}\ (\%) = \frac{\text{moles of GC}_{\text{produced}}}{\text{moles of Gly}_{\text{initial}} - \text{moles of Gly}_{\text{unreacted}}} \times 100 \quad (3)$$

3. Results and discussion

3.1. Catalyst characterisation

3.1.1. Inductively coupled plasma–atomic emission spectroscopy (ICP-AES). Tables 1 and 2 show the compositions of three catalysts determined by ICP-AES.

For the mixed MgO/CaO catalyst, the atomic mass ratio R observed experimentally (Table 1) is higher than the initial mass ratio used to prepare the catalyst (R (Mg/Ca) initial = 1.1). This discrepancy may be due to the heterogeneous distribution of various atoms within the sample as described by Koranian (2024) for the same types of oxide.[35] In the case of the mixed metal oxide KNO_3/CaO, the analysed atomic mass ratio R (K/Ca) (Table 2) is lower than the one used initially (R (K/Ca) initial = 0.12). Additionally, ICP-AES analyses reveal that the catalyst calcined at 700 °C has a higher percentage of potassium atoms and lower abundance of calcium atoms than its counterpart calcined at 900 °C. The calcination temperature is then likely to influence the atomic composition of the minerals. Freeman (1956) reported that potassium nitrate decomposes in the presence of oxygen at elevated temperatures. Above 650 °C, potassium nitrate is converted into potassium nitrite, which subsequently undergoes complete decomposition at around 790 °C.[36] It has been proposed that the potassium atoms released during this process react directly with atmospheric oxygen, leading to the formation of potassium oxides outside the crystalline lattice.[37] The thermogravimetric analysis was carried out on pure KNO_3 (Fig. S1 of the SI). The mass loss of 73% was observed at around 760 °C, therefore confirming these assumptions. As a result, the potassium content decreases progressively with increasing temperature. In contrast, calcium oxide remains stable between 700 and 900 °C.[38] These findings can also explain the variations observed between the atomic compositions measured before calcination and those determined by ICP-AES on the calcined samples.

Table 1 Elementary composition of the MgO–CaO mixed catalyst

	Mg (wt%)	Ca (wt%)	R (Mg/Ca)	R calculated (Mg/Ca)
MgO/CaO	37.5	24.15	1.55	1.2

Table 2 Elementary composition of K–CaO 700 and 900 catalysts

	K (wt%)	Ca (wt%)	R (K/Ca)	R calculated (K/Ca)
KNO_3/CaO 700	2.77	47.16	0.058	0.12
KNO_3/CaO 900	1.10	63.84	0.017	0.12

3.1.2. Structure analysis: X-ray diffraction

Stability of the MgO/CaO catalyst. The XRD pattern of Fig. 2(a) shows a hexagonal ($P\bar{3}m1$) crystalline pattern characteristic of Portlandite, $Ca(OH)_2$ (2θ = 18.1°, 28.7°, 34.2°, 47.3°, 50.8°, 54.5°, 56.3°, 62.8°, and 64.4°). The absence of characteristic CaO (lime) diffraction peaks (2θ = 32.2°, 37.4°, 53.9°, 64.1°, 67.4°) may be attributed the sample's exposure to ambient humidity during analysis. The diffractogram obtained for the calcined MgO sample (Fig. 2(b)) confirms the presence of the cubic crystalline phase ($Fm\text{-}3m$), Periclase with characteristic peaks at 2θ = 36.9°, 42.9°, and 62.3°. The calcined mixed oxide MgO/CaO exhibits three different patterns: cubic CaO, hexagonal $Ca(OH)_2$ and cubic MgO (Fig. 2(c)). Unlike the simple CaO sample, the mixed metal oxide MgO/CaO exhibits the presence of the cubic CaO form. This result confirmed the influence of MgO, particularly Mg^{2+} ions, in the restructuring of the crystal lattice. Indeed, the presence of cubic MgO is supposed to protect the active Ca^{2+} species.[39,40]

The advantage of the mixed MgO/CaO catalyst is to avoid the degradation of calcium oxide into hydroxide/carbonate according to the mechanisms described by eqn (4) and (5)[41,42]:

$$CaCO_{3(s)} \leftrightarrow CaO_{(s)} + CO_{2(g)} \quad (4)$$

$$Ca(OH)_{2(s)} \leftrightarrow CaO_{(s)} + H_2O \quad (5)$$

The catalyst becomes then less sensitive to contact with air (interaction with humidity and CO_2), thus preserving its initial active form.

Effect of calcination temperature on the crystal structure of the KNO_3/CaO catalyst. The mixed oxides, KNO_3/CaO 700 and 900 (Fig. 2(d) and (e)), mainly exhibit a crystal pattern corresponding to Portlandite ($Ca(OH)_2$). For the KNO_3/CaO sample calcined at 700 °C, the peak at 2θ = 37.4° can be attributed to the cubic calcium oxide pattern and the one at 2θ = 29.5° corresponds to the orthorhombic structure of KNO_3 according to Hu *et al.*[34] The decomposition of potassium nitrate is believed to begin at 650 °C[43] following the mechanisms outlined below in eqn (6)–(8). For the mixed oxide calcined at 900 °C, the cubic CaO and orthorhombic KNO_3 patterns are absent, as shown in eqn (7′) and (8′). It can be assumed that KNO_3 reacted with CO_2 and H_2O (air), thus rearranging the crystal structure to form potassium oxide (K_2O, a highly reactive compound) and potassium hydroxide (KOH, a stable molecule).

$$KNO_3 \rightarrow KNO_2 + \frac{1}{2}O_2 \quad (6)$$

$$2KNO_2 \rightarrow K_2O + NO_2 + N_2 \quad (7)$$

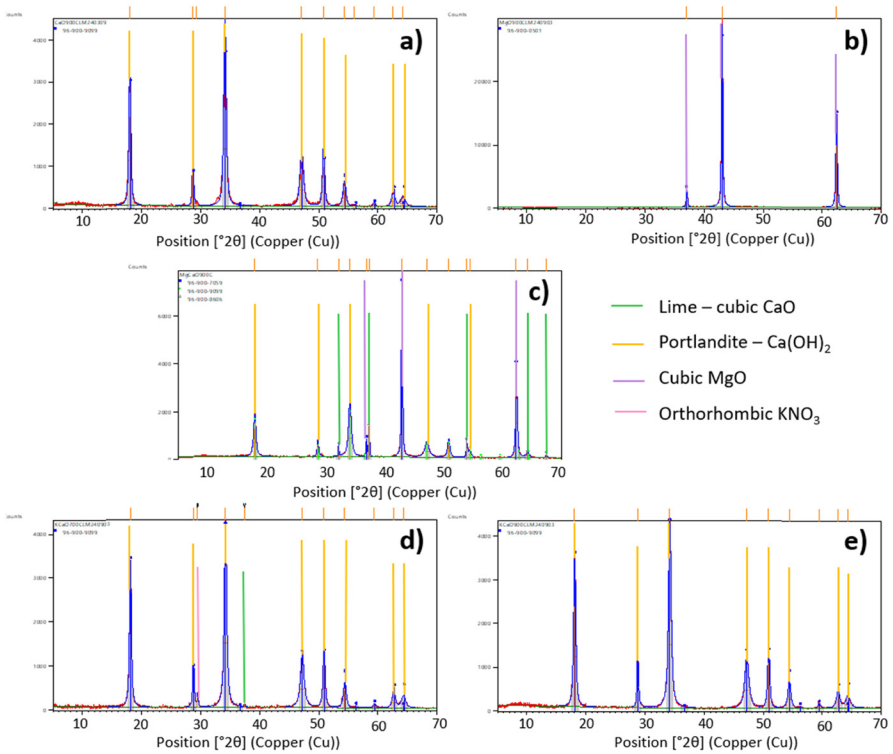

Fig. 2 XRD pattern for calcined catalysts: (a) CaO; (b) MgO; (c) MgO/CaO; (d) KNO_3/CaO 700; (e) KNO_3/CaO 900.

$$\text{followed by } K_2O + H_2O \rightarrow KOH \qquad (7')$$

$$2KNO_2 \rightarrow K_2O + N_2 + \frac{3}{2}O_2 \qquad (8)$$

$$\text{followed by } K_2O + CO_2 \rightarrow KOH \qquad (8')$$

K_2O and KOH can accumulate inside the pores of CaO, resulting in a reduction of the active surface area of the catalyst.[35,44]

This phenomenon could be responsible for the restructuring of the KNO_3/CaO network calcined at 900 °C, thus decreasing its catalytic activity compared to its analogue calcined at 700 °C.

3.1.3. Fourier transform infrared spectroscopy. The Fourier transform infrared spectroscopy was used to identify the characteristic functions of catalyst samples.

Characterization of homogeneous catalysts. For K_2CO_3 and Na_2CO_3, two strong bands were observed in Fig. 3, at 1647 cm^{-1}, 1400 cm^{-3} (K_2CO_3) and 1439 cm^{-1} (Na_2CO_3). These bands are attributed to the typical asymmetric stretching of the C–O bond. The C–O stretching at 1400 cm^{-1} is usually allocated to the aliphatic carbonate function. However, the C–O band at 1647 cm^{-1} is more likely to be assigned to the presence of the bicarbonate group. The same observation was made by Alonso *et al.* (2007) when studying the K_2CO_3/γ Al_2O_3 mixed catalyst.[45] Bicarbonates are formed from carbonates in the presence of water (air) and CO_2 (air) due to the deprotonation of carbonic acid according to eqn (9) and (10). The band at 850 cm^{-1},

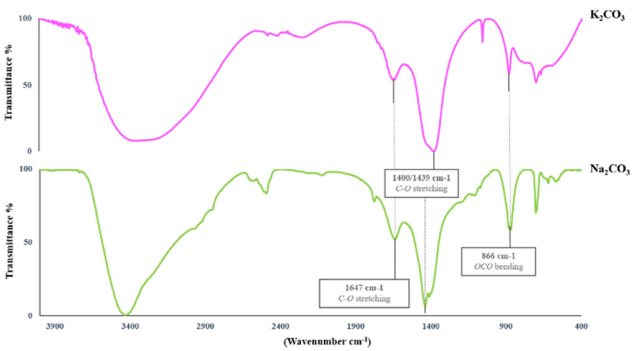

Fig. 3 FT-IR characterization of dried homogeneous catalysts.

corresponding to the bending of the O–C═O group (carboxylate ion),[44] appears in the spectra of both compounds, as shown in Fig. 3. The O–H bond vibrations observed between 3700 and 3000 cm^{-1}, indicate traces of physisorbed water.

$$Na_2CO_3 + H_2O + CO_2 \leftrightarrow 2NaHCO_3 \qquad (9)$$

$$K_2CO_3 + H_2O + CO_2 \leftrightarrow 2KHCO_3 \qquad (10)$$

Characterization of heterogeneous catalysts. The infrared spectra of calcinated metal oxides (MgO and CaO) and mixed oxides (MgO/CaO and KNO_3/CaO 700 and 900) are shown in Fig. 4 and 5. For calcium oxide and mixed catalyst samples, a strong band at 3640 cm^{-1} was observed, which can be attributed to the OH group specific to $Ca(OH)_2$. The formation of the hydroxide species occurs

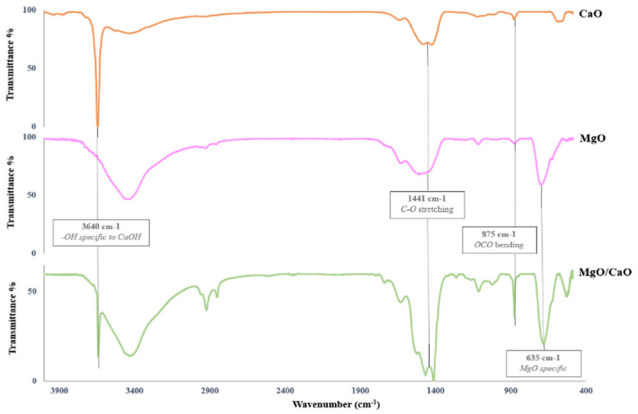

Fig. 4 FT-IR characterisation of the calcined heterogeneous catalysts – CaO, MgO, and MgO/CaO.

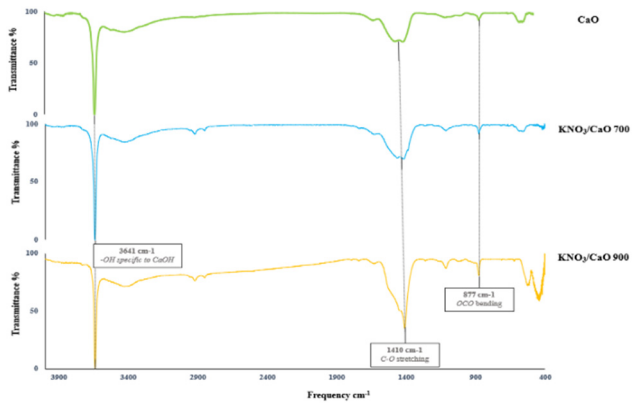

Fig. 5 FT-IR characterisation of the calcined heterogeneous catalysts – CaO, KNO_3/CaO 700, and KNO_3/CaO 900.

when the oxide interacts with water molecules. For the heterogeneous catalysts studied, the signal in the region between 1480 and 1400 cm^{-1} corresponds to the C–O stretching of CO_3^{2-} ions,[44] as observed for homogeneous catalysts. A slight bending band of the OCO group appears at 875 cm^{-1}[44] for CaO, MgO/CaO, KNO_3/CaO 700 and KNO_3/CaO 900. In Fig. 4, MgO displays a band at 635 cm^{-1}, corresponding to a cubic form, as described by Wang *et al.*[46] This vibration is also observed in the mixed oxide MgO/CaO sample. In Fig. 5, the absence of a nitrate ion stretching band around 825 cm^{-1} for the mixed KNO_3/CaO catalysts, indicates that the impregnation was complete as described by Olutoye.[47]

3.1.4. Scanning electron microscopy (SEM). The surface morphology of the different catalysts was analysed by SEM. First, the magnification of the two simple metal oxide catalysts CaO and MgO (Fig. 6), showed heterogeneously sized dispersion crystalline aggregates. Fig. 7 shows CaO particles consisting of stacked crystalline microstructures in the form of smooth cuboids ranging in size from 4 to 16 μm. Metallic oxides often exhibit cuboidal clusters[3] while images of the pure MgO sample (Fig. 6(b) and 8(c)) show spherical structures with rough surfaces.

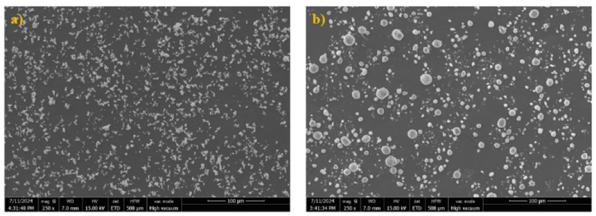

Fig. 6 SEM images (magnification of 250× at 15.00 kV) of CaO (a) and MgO (b).

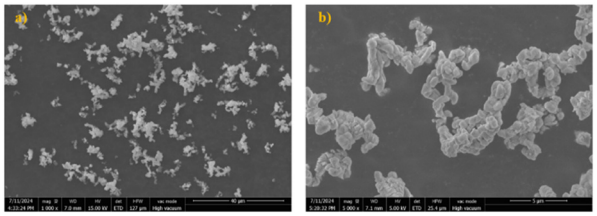

Fig. 7 SEM images of CaO: (a) magnification of 1000× at 15.0 kV; (b) magnification of 5000× at 5.00 kV.

The formation of "bird's nest" shaped crystals typical of the oxide form begins at 100 °C for $MgCO_3$.[48] Zhou *et al.* (2011) highlighted the presence of rough microspheres with rose petal-like surface artifacts, after calcination (500 °C for 3 h) of magnesium oxide.[49] Thereby, as shown in Fig. 8(c) at 3000X magnification, SEM analysis of MgO calcined at 800 °C shows oxide microspheres with similar structures, spheres with rough surfaces (bird's nest or rose petal-covered surfaces as artifacts).

The MgO/CaO catalyst exhibits a heterogeneous dispersion of aggregates with two types of structures: spherical and stacked cuboids of varying sizes, ranging from 2 to 30 μm. The spherical structures are slightly larger and more abundant (Fig. 8(a) and (b)). The crystalline forms of the stacked cuboids and spheres correspond to CaO and MgO, respectively. Unlike

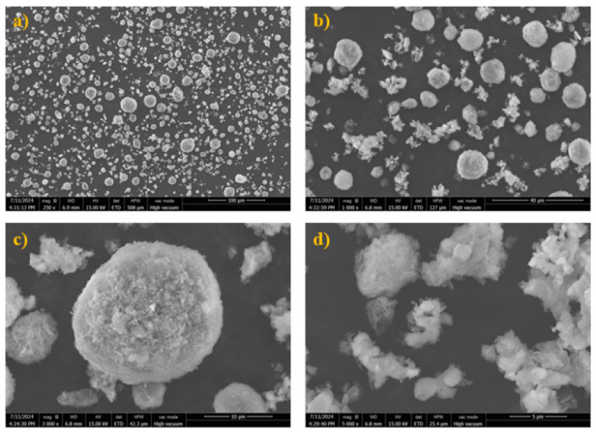

Fig. 8 SEM images of MgO/CaO at 15.00 kV: (a) magnification of 250×; (b) magnification of 1000×; (c) zoomed-in on MgO particles with a magnification of 3000×; (d) zoomed-in on cubic structures with a magnification of 5000×.

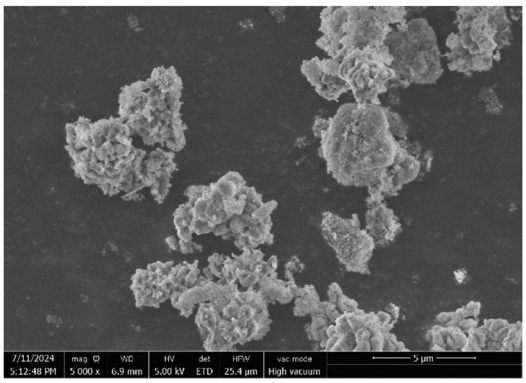

Fig. 9 SEM image of MgO/CaO calcined at 800 °C, zoomed-in on CaO stacking with a magnification of 5000× at 5.00 kV.

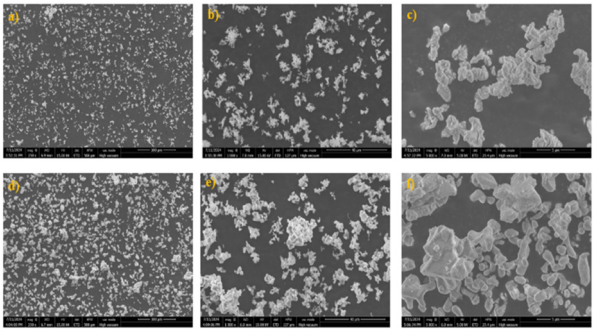

Fig. 10 SEM images (magnification, electron penetration) of KNO_3/CaO calcined at 700 °C; (a) 250×, 15.00 kV; (b) 1000×, 15.00 kV; (c) 5000×, 5 kV and KNO3/CaO calcined at 900 °C; (d) 250×, 15.00 kV; (e) 1000×, 15.00 kV; (d) 5000×, 5.00 kV.

pure CaO, the CaO crystals in the mixed oxide MgO/CaO have a rough surface. This may be due to the deposition of fine MgO particles (Fig. 9) as suggested by Koranian *et al.*[35] Furthermore, deeper electron penetration (15 kV) showed dumbbell-shaped CaO crystals (Fig. 8(d)), a typical structure of oxides as described by Khayoon *et al.*[3] Other crystals are in cubic form within different crystal stacks also showing the presence of an oxide structure as confirmed by Taufiq-Yap.[50]

KNO_3/CaO calcined at 700 °C exhibits structures with homogeneous morphology (Fig. 10(b)), resembling a stack of quasi-laminar sheets or oat flakes (Fig. 10(c)). In contrast, the same compound prepared at 900 °C displays stacked cuboid structures with some dumbbell-shaped crystals (Fig. 10(e)). Some crystals have surface roughness and deposits of small particles of various shapes (Fig. 10(d)). KNO_3/CaO catalysts exhibit homogeneous particle dispersion with larger crystalline aggregates for the catalyst calcined at 900 °C (Fig. 10(a) and (d)). This observation indicates that the size of crystalline particles increases with calcination temperature. Indeed, Hu *et al.* (2012) observed that a high calcination temperature tends to aggregate oxide particles.[34] In general, larger aggregates are not favourable to catalytic activity.

3.1.5. Textural properties – BET analysis. Table 3 gathers BET analysis results for the heterogeneous catalysts.

Table 3 BET analysis results of heterogenous catalysts

	BET surface (m^2 g^{-1})	Total pore volume (cm^3 g^{-1})	Total pore surface area (m^2 g^{-1})	Average pore diameter (nm)
CaO	6.9	0.011	4.9	40.8
MgO	20.6	0.029	22.2	37.1
MgO/CaO	15.2	0.025	17.7	36.2
KNO_3/CaO 700	7.8	0.012	6.6	31.6
KNO_3/CaO 900	3.3	0.005	2.2	36.5

Specific surface area and particle size (BET surface area). The BET surface areas obtained for CaO and MgO calcinated at 800 °C are similar to the values found in the literature for the oxide calcinated at 850 °C, which are 2.7 m^2 g^{-1} and 24.7 m^2 g^{-1}, respectively.[3] For the other catalysts calcined at 800 °C, the values obtained are slightly lower than those reported in the literature: 31.7 m^2 g^{-1} for $Mg_{1.2}Ca_{0.8}O_2$,[3] 11.2 m^2 g^{-1} for Mg–Ca mixed oxide 1 : 1,[35] 11.1 m^2 g^{-1} for KNO_3/CaO,[34] 12.6 m^2 g^{-1} for KNO_3/CaO calcined at 900 °C.[34] The differences between the obtained results and literature data for these samples are probably due to variations in catalyst preparation and analysis conditions. Brief exposure to moisture could cause particle agglomeration, thereby limiting access to the pores.

According to SEM analysis, the particle sizes of the KNO_3/CaO 900 sample were higher than those of KNO_3/CaO 700, (Fig. 10(a) and (d)). This suggests that particle agglomeration is promoted by the calcination temperature, which can explain the decrease in the specific surface area, as previously discussed in the literature.[3,34]

Porosity. The average pore diameters of the catalysts are between 30 and 45 nm (Table 3) indicating that these metal oxides are mesoporous. According to the International Union of Pure and Applied Chemistry (IUPAC), mesoporous materials have an average pore diameter between 2 and 50 nm.[51]

The nitrogen adsorption–desorption isotherms are shown in Fig. S2 of the SI. The five catalysts exhibit the type IV isotherm as well as the typical point B. Such a type of isotherm is linked to mesoporous materials. A slight hysteresis loop is observed for CaO (Fig. S2 of SI (a), MgO (b), MgO/CaO (c) and KNO_3/CaO 900 (e)), indicating that these isotherms could be classified as type IVa. The isotherms of mixed oxide KNO_3/CaO 700 correspond to isotherm type IVb (Fig. S2 of the SI (c) and (d) respectively) because of the missing hysteresis loop. The absence of a hysteresis loop suggests smaller mesopores with fully reversible capillary condensation.[52] This indicates the presence of interconnected pores of varying sizes which may improve the diffusion of the reagents on the catalyst surface, thus enhancing the catalytic activity.[53]

3.1.6. Thermogravimetric analysis (TGA). Fig. 11 shows TAG graphs corresponding to the analysis of four heterogeneous catalysts.

For the four analysed compounds (CaO, KNO_3/CaO 700, KNO_3/CaO 900, and MgO/CaO), three mass losses are observed. The first mass loss between 50 and 100 °C can be associated with the evaporation of undissociated water present in the

samples. The losses range from 3 to 43% depending on the hygroscopicity of the catalyst. For this temperature range, KNO_3/CaO calcined at 900 °C (3% mass loss) shows a lower water mass loss, compared to its counterpart calcined at 700 °C, which loses 43% of its mass. The second mass loss (10% to 20%), taking place between 300 and 500 °C, is associated with the removal of hydroxyl functional groups. The presence of the OH function results from the dissociative chemisorption of water molecules, where the first step is the formation of OH groups on the oxide surface through complexation with cations (Ca^{2+}, Mg^{2+}, and K^{+}).[16] The final mass loss occurs between 600 and 650 °C and corresponds to the dissociation of carbonate groups formed when oxides interact with carbon dioxide from the air.

These results confirm the choice of the calcination temperature for catalyst activation to ensure their oxide form. For the four samples, an activation temperature above 650 °C should lead to only oxide forms.

3.1.7. Basic strength evaluation by the Hammett indicator method. The basic strength of the catalysts was evaluated using the Hammett indicator method. When a colour change occurs in the presence of a given indicator, the basic strength of the catalyst is considered higher than the corresponding Hammett function value (H_).

For the simple oxides, the CaO catalyst did not induce any colour change with the tested indicators, indicating a basic strength lower than H_ = 9.3. MgO caused a colour transition of phenolphthalein from colourless to pink but did not affect 2,4-dinitroaniline, suggesting a basic strength in the range of $9.3 < H_- < 15.0$. A similar behaviour was observed for the mixed KNO_3/CaO 900 catalyst, whose basicity also fell within this interval. The KNO_3/CaO 700 mixed oxide induced a colour change in 2,4-dinitroaniline (from yellow to brown) but not in 4-nitroaniline (H_ = 18.4), indicating a basic strength between $15.0 < H_- < 18.4$. Among all the tested catalysts, the MgO/CaO mixed oxide exhibited the highest basicity, as it changed the colour of 4-nitroaniline (from brown to yellow) but not that of aniline (H_ = 27.0).

Based on the Hammett indicator results, the catalysts can thus be ranked in increasing order of basic strength as follows:

$$CaO < MgO = KNO_3/CaO\ 900 < KNO_3/CaO\ 700 < MgO/CaO.$$

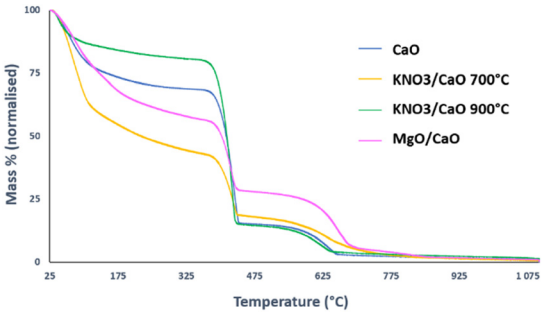

Fig. 11 Thermograms of the heterogenous metal oxide catalyst.

3.2. Catalytic activity: transesterification of glycerol with DEC

The reaction mechanism, Fig. 12, has been reported by different authors.[21,29,54] It involves the exchange of a carbonyl group between an alcohol and a carbonate source, diethyl carbonate in this case. The first step of the heterogenous catalysis reaction mechanism involves proton abstraction by the basic catalyst to form an intermediate glyceroxide anion. Then the latter attacks DEC as a nucleophile followed by the release of the first ethanol molecule. The new intermediate molecule undergoes an intramolecular nucleophilic substitution releasing the second ethanol molecule and forming GC as a final product.

The search for optimal conditions for the transcarbonation reaction studied requires special attention due to its endothermicity (ΔH° = 115.71 kJ mol^{-1}) and its non-spontaneous nature (ΔG° = 13.523 kJ mol^{-1}).[27,55] The reaction equilibrium can be shifted by using one of the reactants in excess and by removing the volatile product. Furthermore, a particular characteristic of the system arises from the non-miscibility of the reactants[27] and the variation of the boiling point of the liquid medium during the reaction.

Two secondary reactions, oligomerisation and glycidol formation can occur according to transcarbonation conditions. Polycarbonate formation is undetectable by the usual analytical methods (FT-IR and GC FID). The formation of these oligomers results in a yellow/brown viscous product,[19] as an indicator of the phenomenon. Oligomerisation is enhanced by the basicity of the catalyst promoting the opening of the GC ring formed.[21] Oligomerization mechanisms lead to complex reactions depending on the involved group (ODO or hydroxyl). This mechanism is triggered when the reaction medium temperature exceeds 120–130 °C. Tests conducted at 130 °C in the presence of a basic catalyst showed evidence of the oligomer formation, as discussed by some authors.[21,23,56] On the other hand, the formation of glycidol, a highly reactive compound, is due to the deprotonation of the primary alcohol group of GC by a strong base followed by an intermolecular nucleophilic substitution causing the GC ring opening. The closure of the epoxy ring is accompanied by the release of a CO_2 molecule.[57,58]

Several catalysts were tested for the transesterification reaction between glycerol and DEC. Glycerol conversion, glycerol carbonate yield and reaction selectivity were calculated for the different catalysts (Tables 4 and 5) based on the chromatograms (Fig. S3 of the SI). Generally, for this type of reaction, the catalyst efficiency requires a moderate base activity. The basic strength is necessary for the first step of the reaction (the abstraction of the primary hydroxyl group proton). In the heterogeneous medium, the catalytic reaction mainly occurs on the surface of the catalyst and the limiting factor is the

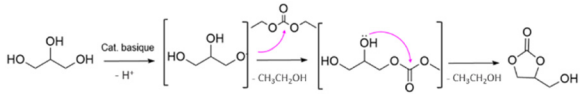

Fig. 12 Mechanism of the transesterification reaction between glycerol and DEC to form glycerol carbonate.

Table 4 Results obtained with homogeneous catalysts

Catalyst	wt%/Gly	Glycerol conversion (%)	GC yield (%)	GC selectivity (%)
Na_2CO_3	5	93 ± 4	58 ± 9	63 ± 12
	10	90 ± 4	54 ± 5	61 ± 3
K_2CO_3	5	90 ± 2	66 ± 11	74 ± 12
	10	89 ± 3	69 ± 9	77 ± 8

Table 5 Results obtained with heterogeneous catalysts

Catalyst	wt%/Gly	Glycerol conversion (%)	GC yield (%)	GC selectivity (%)
CaO	5	27 ± 1	2 ± 1	6 ± 1
	10	46 ± 1	1 ± 1	2 ± 1
MgO	5	41 ± 1	2 ± 1	6 ± 1
	10	43 ± 1	1 ± 1	2 ± 1
MgO/CaO	5	51 ± 2	49 ± 2	97 ± 4
	10	80 ± 4	74 ± 2	93 ± 3
KNO_3/CaO 700	5	92 ± 2	88 ± 2	96 ± 4
	10	93 ± 2	71 ± 2	76 ± 2
KNO_3/CaO 900	5	30 ± 1	2 ± 1	7 ± 1
	10	6 ± 1	4 ± 1	61 ± 1

reagent mass transport from the bulk solution to the catalyst's surface. The choice of CaO core was based on the results obtained for transcarbonation reaction using DMC and for transesterification leading to biodiesel.[23,40,59–62]

In Table 4, the results obtained for the reactions with two earth metal carbonates showed high glycerol conversions. However, the selectivity of the reaction was limited due to the formation of carbonate oligomers observed as a brown deposit on the macroporous resin. It was found that after one hour of reaction, K_2CO_3 behaved more like a heterogeneous catalyst, due to the change in the medium composition. Since the separation of the K_2CO_3 catalyst by centrifugation was incomplete, the use of a cationic exchange resin was necessary, as for the homogeneous Na_2CO_3 catalyst.

Table 5 displays the results obtained from experimental tests with the selected catalysts. It should be noted that the glycerol carbonate yields (and the resulting selectivities) in Table 5 do not take into account the glycerol carbonate trapped with the catalyst grains separated from the liquid phase by filtration. Calculations have shown that the yields of GC were underestimated by 5–16% for experiments involving the MgO/CaO and KNO_3/CaO 700 catalysts, meaning that the actual selectivities are higher than the reported values (Table S1 of the SI). The estimation was done by the mass balance carried out from the GC synthesis and its work-up. An example of the mass balance for the KNO_3/CaO 700 5% wt/Gly catalyst is shown in Fig. S4 of the SI.

For the single metal heterogeneous oxides, CaO and MgO, we observe low GC yields. This result can be explained by the partial deactivation of the CaO catalyst by interactions with H_2O and CO_2.[19] According to XRD analysis, the only phase present in the CaO catalyst is the hexagonal $Ca(OH)_2$ hydrated phase. Moreover, the FTIR spectrum of the catalyst after the reaction shows the presence of non-dissociated water on the catalyst's surface. Furthermore, the low basicity of the CaO catalyst corroborates the average performance of these catalysts. For MgO, we could expect a lower basic strength, if we compare alkaline earth metals (group 2A – second column of the periodic table) with alkali metals (group 1A – first column of the periodic table). This assumption was confirmed by the low basicity of MgO catalytic sites ($9.3 < H_- < 15$).

The best catalytic performances were observed for mixed heterogeneous catalysts (MgO/CaO, 10% loading and KNO_3/CaO 700, 5% loading) with GC yields of 74% and 88% respectively. For MgO/CaO, when using the higher loading, a quantitative glycerol conversion and a good GC selectivity were obtained.

These results are in agreement with previous work using mixed catalysts when DMC was employed as a carbonate source. Khayoon *et al.* (2013), reported a 100% GC yield with MgO/CaO, at 70 °C after 90 min.[3] Likewise, Hu *et al.* (2025) obtained an 85% GC yield (at 70 °C after 2 h) with a catalyst based on the KNO_3/CaO 700 catalyst.[34]

In the case of the mixed heterogeneous KNO_3/CaO 700 catalyst, we can observe that the lower catalyst loading provides a high GC selectivity, limiting the glycidol formation as a secondary product (not detected by GC). The KNO_3/CaO 700 catalyst shows orthorhombic KNO_3 and cubic CaO structures according to XRD analysis (Fig. 2(d)). Additionally, its high basic strength ($15 < H_- < 18.4$) can explain the catalytic activity as well as its crystalline structure.

The mixed KNO_3/CaO 900 catalyst displayed a very low catalytic activity at both loadings, probably due to the low measured basicity ($9.3 < H_- < 15$) and the particle agglomeration observed in the SEM images (Fig. 10).

The results therefore confirm that coupling the active calcium core with another metal component as a support, can protect the active sites from air. Moreover, the association of the active CaO core with Mg^{2+} and K^+ led to a higher specific surface, while retaining mesoporous characteristics (average pore sizes in Table 3).

Finally, related homogeneous catalysts (alkali metals carbonates) showed a lack of selectivity for transcarbonation of glycerol with DEC. Furthermore, the use of homogeneous catalysts comes with significant challenges in terms of separation and reusability, especially at larger scales. Heterogeneous base catalysis overcomes the limitations of homogeneous catalysis, and provides a more environmentally friendly alternative.[63] It should be noted that studying the morphology of heterogeneous catalysts is necessary to understand the surface interactions between the reactants and the catalyst.

The selected mixed oxides can be easily separated from the final product and potentially reactivated to be reused.

4. Conclusions

This study highlights the feasibility of the transcarbonation reaction of glycerol with DEC in mild conditions and quantitative yields, thanks to two heterogeneous mixed metal oxide

catalysts, MgO/CaO, (10%) and KNO_3/CaO 700 (5%). The results have demonstrated the advantages of using these easily prepared mixed oxides. These mixed oxides exhibit mesoporous characteristics and high basic basicity (H_ > 15) making them suitable for the transcarbonation reaction. The superior performance of KNO_3/CaO calcinated at 700 °C can be attributed to its stability in air and its crystalline form.

The different analyses confirmed that the calcination temperature played a significant role in catalytic activity, as it influences the crystal lattice structure and the morphology of particles. We identified a minimum calcination temperature (650 °C for the studied oxides) and a critical calcination temperature to be considered.

The results of this work open up new perspectives and demonstrate strong potential for the development of a glycerol transcarbonation process using DEC as a carbonate source, made possible by the use of heterogeneous catalysts based on mixed metal oxides. These catalysts, easy to prepare and efficient under mild conditions, promote the development of novel production processes that optimize yields while minimizing environmental impact. In the future, the integration of process intensification strategies such as reactive distillation, membrane reactors or advanced heating technologies could significantly enhance productivity, selectivity, and energy efficiency. These approaches offer a promising path toward the industrial scale-up of an environmentally friendly process in line with the principles of green chemistry and sustainable development.

Author contributions

Linda Miturova: conceptualisation, data curation, methodology, formal analysis, investigation, visualisation, writing – original draft. Ivonne Rodriguez-Donis: conceptualisation, funding acquisition, methodology, supervision, validation, writing – review and editing. Pascale de Caro: conceptualisation, funding acquisition, methodology, supervision, validation, writing – review and editing.

Conflicts of interest

There are no conflicts to declare.

Data availability

The data supporting this article have been included as part of the supplementary information (SI). Supplementary information: precisions about results of catalyst screening and example of mass balance calculations. See DOI: https://doi.org/10.1039/d5nj03530a.

Acknowledgements

This work was supported by the French state through the National Research Agency under the Program for Future Investments bearing the reference ANR-18-EURE-0021. The financial support was provided by the network Carnot 3BCAR (GreenCarGly program) and the French Ministry of Higher Education and Research (MESR).

References

1 I. Ambat, V. Srivastava and M. Sillanpää, Recent advancement in biodiesel production methodologies using various feedstock: A review, *Renewable Sustainable Energy Rev.*, 2018, **90**, 356–369.
2 M. E. Kibar, L. Hilal, B. T. Çapa, B. Bahçıvanlar and B. B. Abdeljelil, Assessment of Homogeneous and Heterogeneous Catalysts in Transesterification Reaction: A Mini Review, *ChemBioEng Rev.*, 2023, **10**(4), 412–422.
3 M. S. Khayoon and B. H. Hameed, $Mg_{1+x}Ca_{1-x}O_2$ as reusable and efficient heterogeneous catalyst for the synthesis of glycerol carbonate via the transesterification of glycerol with dimethyl carbonate, *Appl. Catal., A*, 2013, **466**, 272–281.
4 M. O. Sonnati, S. Amigoni, E. P. T. de Givenchy, T. Darmanin, O. Choulet and F. Guittard, Glycerol carbonate as a versatile building block for tomorrow: synthesis, reactivity, properties and applications, *Green Chem.*, 2013, **15**(2), 283–306.
5 P. de Caro, M. Bandres, M. Urrutigoïty, C. Cecutti and S. Thiebaud-Roux, Recent Progress in Synthesis of Glycerol Carbonate and Evaluation of Its Plasticizing Properties, *Front. Chem.*, 2019, 7.
6 M. Salari, J. C. Varela, H. Zhang and M. W. Grinstaff, Sustainable glycerol carbonate electrolytes for Li-ion supercapacitors: performance evaluation of butyl, benzyl, and ethyl glycerol carbonates, *Mater. Adv.*, 2021, **2**(18), 6049–6057.
7 P. Prete, S. Trano, P. Zaccagnini, L. Fagiolari, J. Amici and A. Lamberti, *et al.*, Glycerol carbonate and solketal carbonate as circular economy bricks for supercapacitors and potassium batteries, *ChemSusChem*, 2024, **17**, e202401636.
8 N. Rozulan, S. A. Halim, N. Razali and S. S. Lam, A review on direct carboxylation of glycerol waste to glycerol carbonate and its applications, *Biomass Convers. Biorefin.*, 2022, **12**(10), 4665–4682.
9 R. Valentin, M. Alignan, G. Giacinti, F. N. R. Renaud, B. Raymond and Z. Mouloungui, Pure short-chain glycerol fatty acid esters and glycerylic cyclocarbonic fatty acid esters as surface active and antimicrobial coagels protecting surfaces by promoting superhydrophilicity, *J. Colloid Interface Sci.*, 2012, **365**(1), 280–288.
10 S. Holmiere, R. Valentin, P. Maréchal and Z. Mouloungui, Esters of oligo-(glycerol carbonate-glycerol): New biobased oligomeric surfactants, *J. Colloid Interface Sci.*, 2017, **487**, 418–425.
11 B. Nohra, L. Candy, J. F. Blanco, C. Guerin, Y. Raoul and Z. Mouloungui, From Petrochemical Polyurethanes to Biobased Polyhydroxyurethanes, *Macromolecules*, 2013, **46**(10), 3771–3792.
12 D. M. Fitzgerald, H. Zhang, C. Bordeianu, Y. L. Colson and M. W. Grinstaff, Synthesis of Polyethylene Glycol–Poly(glycerol

carbonate) Block Copolymeric Micelles as Surfactant-Free Drug Delivery Systems, *ACS Macro Lett.*, 2023, **12**(7), 974–979.
13 S. Franklin, Carbonate-haloformate of glycerol and method of producing same [Internet], 2446145, 1948, Available from: https://www.freepatentsonline.com/2446145.html.
14 A. Behr, J. Eilting, K. Irawadi, J. Leschinski and F. Lindner, Improved utilisation of renewable resources: New important derivatives of glycerol, *Green Chem.*, 2008, **10**(1), 13–30.
15 S. Nomanbhay, M. Y. Ong, K. W. Chew, P. L. Show, M. K. Lam and W. H. Chen, Organic Carbonate Production Utilizing Crude Glycerol Derived as By-Product of Biodiesel Production: A Review, *Energies*, 2020, **13**(6), 1483.
16 G. D. Yadav and P. A. Chandan, A green process for glycerol valorization to glycerol carbonate over heterogeneous hydrotalcite catalyst, *Catal. Today*, 2014, **237**, 47–53.
17 S. Claude, Z. Mouloungui, J. W. Yoo and A. Gaset Procédé de fabrication de carbonate de glycérol. EP0955298A1, 1999. Available from: https://patents.google.com/patent/EP0955298A1/fr.
18 R. A. van Dam, A. C. Hogan, C. D. McCullough, M. A. Houston, C. L. Humphrey and A. J. Harford, Aquatic toxicity of magnesium sulfate, and the influence of calcium, in very low ionic concentration water, *Environ. Toxicol. Chem.*, 2010, **29**(2), 410–421.
19 J. R. Ochoa-Gómez, O. Gómez-Jiménez-Aberasturi, B. Maestro-Madurga, A. Pesquera-Rodríguez, C. Ramírez-López and L. Lorenzo-Ibarreta, *et al.*, Synthesis of glycerol carbonate from glycerol and dimethyl carbonate by transesterification: Catalyst screening and reaction optimization, *Appl. Catal., A*, 2009, **366**(2), 315–324.
20 P. U. Okoye, A. Z. Abdullah and B. H. Hameed, Glycerol carbonate synthesis from glycerol and dimethyl carbonate using trisodium phosphate, *J. Taiwan Inst. Chem. Eng.*, 2016, **68**, 51–58.
21 G. Rokicki, P. Rakoczy, P. Parzuchowski and M. Sobiecki, Hyperbranched aliphatic polyethers obtained from environmentally benign monomer: glycerol carbonate, *Green Chem.*, 2005, **7**(7), 529.
22 G. Pradhan and Y. C. Sharma, Green synthesis of glycerol carbonate by transesterification of bio glycerol with dimethyl carbonate over Mg/ZnO: A highly efficient heterogeneous catalyst, *Fuel*, 2021, **284**, 118966.
23 W. Praikaew, W. Kiatkittipong, F. Aiouache, V. Najdanovic-Visak, K. Ngaosuwan and D. Wongsawaeng, *et al.*, Process and Energy Intensification of Glycerol Carbonate Production from Glycerol and Dimethyl Carbonate in the Presence of Eggshell-Derived CaO Heterogeneous Catalyst, *Energies*, 2021, **14**(14), 4249.
24 M. A. Pacheco and C. L. Marshall, Review of Dimethyl Carbonate (DMC) Manufacture and Its Characteristics as a Fuel Additive, *Energy Fuels*, 1997, **11**(1), 2–29.
25 I. Patraşcu, C. S. Bîldea and A. A. Kiss, Novel eco-efficient reactive distillation process for dimethyl carbonate production by indirect alcoholysis of urea, *Front. Chem. Sci. Eng.*, 2022, **16**(2), 316–331.
26 Z. Zhang, H. Xu, Q. Zhang, A. Zhang, Y. Li and W. Li, Separation of methanol + dimethyl carbonate azeotropic mixture using ionic liquids as entrainers, *Fluid Phase Equilib.*, 2017, **435**, 98–103.
27 J. Liu, D. Pan, Q. Zhang, Y. Guan and B. Yang, Liquid-liquid equilibrium of immiscible systems involved in glycerol transesterification with diethyl carbonate, *Fluid Phase Equilib.*, 2022, **558**, 113455.
28 P. Tundo, F. Aricò, A. E. Rosamilia, M. Rigo, A. Maranzana and G. Tonachini, Reaction of dialkyl carbonates with alcohols: Defining a scale of the best leaving and entering groups, *Pure Appl. Chem.*, 2009, **81**(11), 1971–1979.
29 M. G. Alvarez, A. M. Segarra, S. Contreras, J. E. Sueiras, F. Medina and F. Figueras, Enhanced use of renewable resources: Transesterification of glycerol catalyzed by hydrotalcite-like compounds, *Chem. Eng. J.*, 2010, **161**(3), 340–345.
30 M. G. Álvarez, M. Plíšková, A. M. Segarra, F. Medina and F. Figueras, Synthesis of glycerol carbonates by transesterification of glycerol in a continuous system using supported hydrotalcites as catalysts, *Appl. Catal., B*, 2012, **113–114**, 212–220.
31 R. L. Souza Júnior, T. M. Rossi, C. Detoni and M. M. V. M. Souza, Glycerol carbonate production from transesterification of glycerol with diethyl carbonate catalyzed by Ca/Al-mixed oxides derived from hydrocalumite, *Biomass Convers. Biorefin.*, 2023, **13**(2), 661–673.
32 Y. Wu, X. Song, F. Cai and G. Xiao, Synthesis of glycerol carbonate from glycerol and diethyl carbonate over Ce-NiO catalyst: The role of multiphase Ni, *J. Alloys Compd.*, 2017, **720**, 360–368.
33 S. C. Andola, A. Pandey, A. C. Kothari, G. Singh, A. Singh and R. Malik, Green Synthesis of Glycerol Carbonate from Glycerol Over Prepared Sodium Aluminate Catalysts by Spray Drying, *Catal. Lett.*, 2025, **155**(7), 1–15.
34 K. Hu, H. Wang, Y. Liu and C. Yang, KNO3/CaO as cost-effective heterogeneous catalyst for the synthesis of glycerol carbonate from glycerol and dimethyl carbonate, *J. Ind. Eng. Chem.*, 2015, **28**, 334–343.
35 P. Koranian, A. K. Dalai and R. Sammynaiken, Structural study of mixed metal oxide catalysts comprising Mg, Ca, and Al used for upgrading biodiesel byproduct glycerol to glycerol carbonate, *Appl. Catal., A*, 2024, **679**, 119727.
36 E. S. Freeman, The Kinetics of the Thermal Decomposition of Potassium Nitrate and of the Reaction between Potassium Nitrite and Oxygen1a, *J. Am. Chem. Soc.*, 1957, **79**(4), 838–842.
37 C. M. Kramer, Z. A. Munir and J. V. Volponi, Screening tests of sodium nitrate and potassium nitrate decomposition, *Sol. Energy*, 1982, **29**(5), 437–439.
38 J. R. Nelson, R. J. Needs and C. J. Pickard, Calcium peroxide from ambient to high pressures, *Phys. Chem. Chem. Phys.*, 2015, **17**(10), 6889–6895.
39 S. Arora, V. Gosu, U. K. A. Kumar, T. C. Zhang and V. Subbaramaiah, A novel Ce-CaO/MgO catalyst derived from marble waste through green synthesis route for glycerol carbonate synthesis, *React. Kinet., Mech. Catal.*, 2021, **132**(2), 839–858.

40 A. Kaur and A. Ali, Surface-Modified CaO Catalyst for the Production of Glycerol Carbonate, *ChemistrySelect*, 2021, **6**(24), 6102–6114.
41 R. Barker, The reactivity of calcium oxide towards carbon dioxide and its use for energy storage, *J. Appl. Chem. Biotechnol.*, 1974, **24**(4–5), 221–227.
42 D. R. Glasson, Reactivity of lime and related oxides. I. Production of calcium oxide, *J. Appl. Chem.*, 1958, **8**(12), 793–797.
43 Y. H. Sun, L. B. Sun, T. T. Li and X. Q. Liu, Modulating the Host Nature by Coating Alumina: A Strategy to Promote Potassium Nitrate Decomposition and Superbasicity Generation on Mesoporous Silica SBA-15, *J. Phys. Chem. C*, 2010, **114**(44), 18988–18995.
44 Y. T. Algoufi, G. Kabir and B. H. Hameed, Synthesis of glycerol carbonate from biodiesel by-product glycerol over calcined dolomite, *J. Taiwan Inst. Chem. Eng.*, 2017, **70**, 179–187.
45 D. M. Alonso, R. Mariscal, R. Moreno-Tost, M. D. Z. Poves and M. L. Granados, Potassium leaching during triglyceride transesterification using K/γ-Al2O3 catalysts, *Catal. Commun.*, 2007, **8**(12), 2074–2080.
46 Y. Wang, Y. Chen, C. Liu, F. Yu, Y. Chi and C. Hu, The effect of magnesium oxide morphology on adsorption of U(VI) from aqueous solution, *Chem. Eng. J.*, 2017, **316**, 936–950.
47 M. A. Olutoye, S. C. Lee and B. H. Hameed, Synthesis of fatty acid methyl ester from palm oil (Elaeis guineensis) with Ky(MgCa)2xO3 as heterogeneous catalyst, *Bioresour. Technol.*, 2011, **102**(23), 10777–10783.
48 Q. Chen, T. Hui, H. Sun, T. Peng and W. Ding, Synthesis of magnesium carbonate hydrate from natural talc, *Open Chem.*, 2020, **18**(1), 951–961.
49 J. Zhou, S. Yang and J. Yu, Facile fabrication of mesoporous MgO microspheres and their enhanced adsorption performance for phosphate from aqueous solutions, *Colloids Surf., A*, 2011, **379**(1), 102–108.
50 Y. H. Taufiq-Yap, H. V. Lee, R. Yunus and J. C. Juan, Transesterification of non-edible *Jatropha curcas* oil to biodiesel using binary Ca–Mg mixed oxide catalyst: Effect of stoichiometric composition, *Chem. Eng. J.*, 2011, **178**, 342–347.
51 R. L. Burwell Jr, Manual of symbols and terminology for physicochemical quantities and units–appendix II heterogeneous catalysis, *Advances in Catalysis*, Academic Press, vol. 26, 1977, pp. 351–392.
52 I. Catalin, O. Verdes and M. Suba, Nitrogen Sorption Measurements and Thermal Analysis Techniques, in *Microbial Electrochemical Technologies*, John Wiley & Sons, Ltd, 2023, p. 229–244, Available from: https://onlinelibrary.wiley.com/doi/abs/10.1002/9783527839001.ch8.
53 A. Taiswa, R. L. Maglinao, J. M. Andriolo, S. Kumar and J. L. Skinner, Electrospun Pt-TiO2 nanofibers Doped with HPA for Catalytic Hydrodeoxygenation, *Sci. Rep.*, 2024, **14**(1), 24706.
54 Y. Ji, Recent Development of Heterogeneous Catalysis in the Transesterification of Glycerol to Glycerol Carbonate, *Catalysts*, 2019, **9**(7), 581.
55 J. Zhang, Y. Wu, X. Song, S. Xu, S. Li and Y. Zhu, *et al.*, Thermodynamic and kinetic studies for synthesis of glycerol carbonate from glycerol and diethyl carbonate over Ce–NiO catalyst, *Chem. Pap.*, 2018, **72**(11), 2909–2919.
56 G. Pradhan and Y. C. Sharma, Green synthesis of glycerol carbonate by transesterification of bio glycerol with dimethyl carbonate over Mg/ZnO: A highly efficient heterogeneous catalyst, *Fuel*, 2021, **284**, 118966.
57 J. R. Ochoa-Gómez, O. Gómez-Jiménez-Aberasturi, C. Ramírez-López and B. Maestro-Madurga, Synthesis of glycerol 1,2-carbonate by transesterification of glycerol with dimethyl carbonate using triethylamine as a facile separable homogeneous catalyst, *Green Chem.*, 2012, **14**(12), 3368.
58 D. J. Darensbourg and A. D. Yeung, Kinetics and thermodynamics of the decarboxylation of 1,2-glycerol carbonate to produce glycidol: computational insights, *Green Chem.*, 2014, **16**(1), 247–252.
59 A. Bazargan, M. D. Kostić, O. S. Stamenković, V. B. Veljković and G. McKay, A calcium oxide-based catalyst derived from palm kernel shell gasification residues for biodiesel production, *Fuel*, 2015, **150**, 519–525.
60 F. S. H. Simanjuntak, T. K. Kim, S. D. Lee, B. S. Ahn, H. S. Kim and H. Lee, CaO-catalyzed synthesis of glycerol carbonate from glycerol and dimethyl carbonate: Isolation and characterization of an active Ca species, *Appl. Catal., A*, 2011, **401**(1), 220–225.
61 A. Laca, A. Laca and M. Díaz, Eggshell waste as catalyst: A review, *J. Environ. Manage.*, 2017, **197**, 351–359.
62 P. L. Boey, G. P. Maniam and S. A. Hamid, Performance of calcium oxide as a heterogeneous catalyst in biodiesel production: A review, *Chem. Eng. J.*, 2011, **168**(1), 15–22.
63 N. Kaur and N. Banik, Industrial Applications of Solid Base Catalysis, in *Solid Base Catalysts*, John Wiley & Sons, Ltd, 2024, pp. 169–231. Available from: https://onlinelibrary.wiley.com/doi/abs/10.1002/9783527846719.ch7.